Heat Input Effect on Microstructure and Mechanical Properties in Shielded Metal Arc Welding of Dissimilar AISI 316L/St-37 Steel

M. Ahangaryan [1] , M. Jafarzadegan *[2], R. Taghiabadi [3]

Department of Materials science and Metallurgy, faculty of engineering, Imam Khomeini International University (IKIU), Qazvin, Iran.

Abstract

Joining of stainless steels to carbon steels is one of the most widely used types of dissimilar joints. In this research, the microstructure and mechanical properties of dissimilar shielded metal arc welding of austenitic stainless steel AISI 316L to carbon steel St-37 is studied. This joining has made by E316L electrode and three heat inputs of 0.72, 0.84 and 1.0 kJ/mm. The microstructure of the joints was characterized by optical and scanning electron microscopy. The mechanical properties of the joints were evaluated by tensile and microhardness tests. The solidification microstructure of the weld metals contained mainly austenite and some skeletal delta ferrite. There was an epitaxial growth at the interface of the weld metal with the AISI 316L steel HAZ, and at the interface of the weld metal with the St-37 HAZ, there is an un-etched narrow area which is suggested to have austenitic-martensitic structure. The results of hardness tests showed that the hardness of the interface of the weld metal with the St-37 steel was maximum which is attributed to the formation of the martensitic narrow band. The longitudinal tensile results showed that the increasing of the heat input decreaes the tensile strength and increases the elongation of the joints.

Keywords: St-37 steel; AISI 316L stainless steel; Dissimilar welding; Microstructure; Tensile properties.

1. Introduction

Dissimilar welding is frequently used to join stainless steels to other materials. This technique is usually used where changes in mechanical properties or in performance are required. For example, austenitic stainless steel piping is usually used to transport steam at high temperatures in the power plants. These steels can be replaced by low carbon steels under certain temperature, which have a lower price [1)]. Dissimilar welds of low alloy steel and stainless steel are widely employed in oil, gas and power generating industries, especially in coolant systems [2, 3)]. This kind of dissimilar welding results in a number of significant metallurgical difficulties, such as solidification and hydrogen cracking and formation of carbide and brittle phases, which can cause unexpected component failure [4)].

So far, several researchers have investigated this joints using different welding methods including both fusion and solid state welding. Celik and Alsaran investigated the joining of AISI 304 stainless steel to St37-2 low carbon steel using the gas tungsten arc welding (GTAW) process with an austenitic filler metal and reported the extreme hardness increasing in the HAZ regions of the austenitic–ferritic dissimilar metal joint [1)]. Reddy

*Corresponding author
Email:jafarzadegan@eng.ikiu.ac.ir
Address: Department of Materials science and Metallurgy, faculty of engineering, Imam Khomeini International University (IKIU), Qazvin, Iran.
1. M.Sc
2. Assistant Professor
3. Associate Professor

et al. used the GTAW to join stainless steel 316 to low alloy steel 4140 with and without the filler metal. They suggested that the maximum hardness in the HAZ of steel 4140 is due to the formation of martensite [5]. Khalifeh et al. used GTAW process for joining AISI 304L to St37 steels. They stated that ER309L and ER316L filler metals have a good combination of mechanical and metallurgical properties [6]. Torkamany et al. reported the varying microstructures form austenite-ferrite-martensite to fully martensite in laser spot welding of low carbon and austenitic stainless steel [7]. However, laser welding is expensive and causes the formation of martensite because due to the rapid cooling [8]. Arivazhagan et al. has produced sound welds between AISI 304 and AISI 4140 steels by GTAW and Friction welding, but they observed brittle fracture [9]. The precipitation of $Cr_{23}C_6$ and Cr_7C_3 at the weld interface of carbon steel and austenitic stainless has also been reported [10]. Khosrovaninezhad et al. also investigated the mechanical properties of the dissimilar austenitic stainless steel 316 to St-37 steel joint using FSW. They reported that although the diffusion of alloying elements occurred, but no intermetallic compounds was observed. The reason for not forming these compounds was a very low exposure time at high temperatures [11].

Among different welding methods, shielded metal arc welding (SMAW) is a versatile and available method with a low cost, and it is widely used for fabrication and repair of the welds in the industries [12]. One of the most important factors which affects the microstructure and mechanical properties in the SMAW, is the heat input. With controlling the heat input, the formation of brittle phases is avoided and sound welds with appropriate properties is achievable. Welding heat input is an important factor that affects the microstructure and mechanical properties in the fusion welding processes. The aim of this study is achieving sound welds and investigating the microstructure and mechanical properties of St-37 carbon steel to AISI 316L austenitic stainless steel joints produced by different heat inputs.

2. Materials and Methods

In the present work, AISI 316L and St-37 steel plates were butt-jointed using SMAW with E316L electrode. The thickness of the plates was 3 mm. The chemical composition of the base metals (BMs) and the electrode is presented in table 1.

The plates were welded with different currents of 90, 100, and 115 A. The welding parameters and calculated heat inputs (H.I.) are listed in Table 2. The heat input is calculated using Eq. (1) in which I, V, and S are current, voltage, and speed of the welding; respectively. The η is efficiency which is considered about 80% [13].

$$H.I. = \frac{\eta IV}{S} \qquad \text{Eq. (1)}$$

Due to the large difference in thermal conductivty between steels AISI 316 and St-37, the St-37 plates were preheated at 150 °C before welding according to the ASME [14]. The preheating of the carbon steel

Table 1. The chemical composition of the BMs and the electrode (wt.%).

Element	C	Ni	Cr	Mo	Mn	Si	P	S	Cu	Fe
AISI 316L	0.027	12.16	17.3	2.37	1.56	0.89	0.005	0.04	0.236	Bal.
St-37	0.08	0.043	0.066	0.044	0.181	0.02	0.024	0.044	0.024	Bal.
E316L	0.02	11.7	19.4	2.5	1.33	0.73	0.029	0.016	-	Bal.

Table 2. The welding parameters and calculated heat inputs.

Sample	Current (A)	Volt (V)	Welding speed ($mm\ s^{-1}$)	Heat input ($kJ\ mm^{-1}$)
1	90	18	1.8	0.72
2	100	21	2	0.84
3	115	24	2.2	1.0

decreases the distortion. Preheating of carbon steel was also performed to prevent possible hydrogen cracking which may occur in carbon steels. It is recommended that the weld area and the consumables must be dry before welding in dissimilar welding of carbon to stainless steels.

The metallographic samples were ground by SiC papers and polished with a diamond paste and followed by etching with 2% Nital (2% HNO_3 + 98% alcohol) and Marble's reagent (50 ml HCl + 10 g $CuSO_4$ + 50 ml H_2O)to reveal the microstructure of St-37 and AISI 316 steels; respectively. The grain size was measured with mean linear intercept method and area fraction of the delta ferrite were measured using ImageJ software.

Longitudinal and transversal tensile samples were prepared according to ASTM E8M-99 standard (sub-size specimens). The tensile tests were conducted by Zwick/Roell Z100 device at the crosshead speed of 5 mm min^{-1}. The fracture surfaces of samples were also examined by SEM (AIS2300C). The Vickers hardness of the samples was measured according to ASTM-E384-05a by HVS-1000 hardness device. The hardness load was 100 g with the dwell time of 15 s.

3. Results and Discussion

3.1. Microstructure

The SEM micrograph of St-37 steel BM is shown in Fig. 1. The microstructure consists of equiaxed ferrite grains with a mean 15 ± 2 μm diameter and the pearlite (P) lamellar and some grain boundary cementite particles.

Fig. 2(a) shows the Fe-C diagram and different HAZ parts of the specimen welded with 100 A. The HAZ microstructure of the carbon steel can be divided into essentially three regions: partially grain refining, grain refining, and grain-coarsening regions (regions B, C, and D). The maximum temperatures at these regions are indicated in the phase diagram. The BM is exposed to the temperatures under the eutectoid temperature and remains almost unchanged. The partially grain refining region (B) is subjected to a peak temperature just above the effective lower critical temperature, Ac1. In this region, the prior P colonies transform to austenite (γ) and expand slightly into the prior ferrite (F) colonies upon heating to above Ac1 and then decompose into extremely fine grains of P and F during cooling. The prior F colonies are almost unaffected. The average ferrite size in this area is 10 ± 2 μm. The grain refining region (C) is subjected to a peak temperature just above the effective upper critical temperature Ac_3, thus allowing austenite grains to nucleate. Such austenite grains decompose into small P and ferrite grains during subsequent cooling. The average ferrite size in this area is 9 ± 3 μm. The grain-coarsening region (D) has an average ferrite size of 83 ± 11 μm, because it is subjected to a peak temperature well above Ac_3, thus allowing austenite grains to grow. The high cooling rate and large grain size encourage the ferrite to form side plates from the grain boundaries, which are called Widmanstatten ferrite [13]. There are many small cementite particles dispersed inside (marked by black arrows in Fig. 2d) and at the ferrite boundaries (marked by white arrows). The other specimens have the same HAZ microstructure. By increasing the heat input, there is only a little grain size increasing in the different parts of St-37 HAZ. This is because the similar regions experience the same peak temperatures but exposure times are a little different due to the different cooling rates.

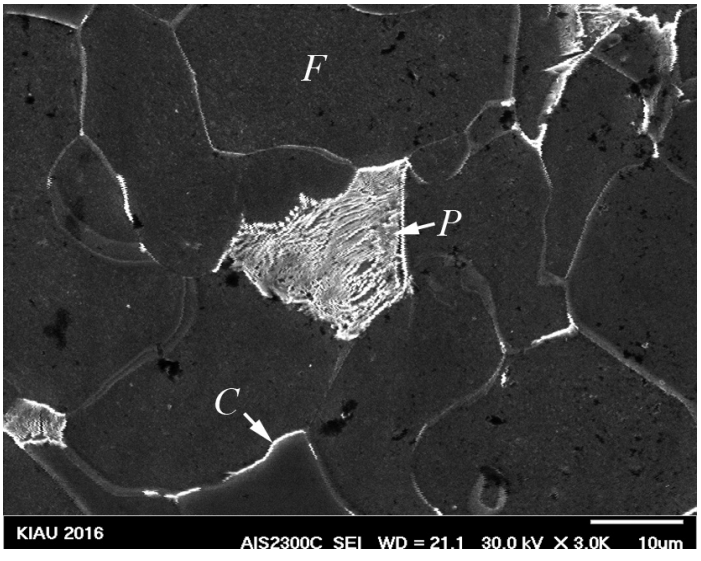

Fig. 1. SEM micrograph of the St-37 BM. F: Ferrite, P: Pearlite, C: Grain boundary cementite.

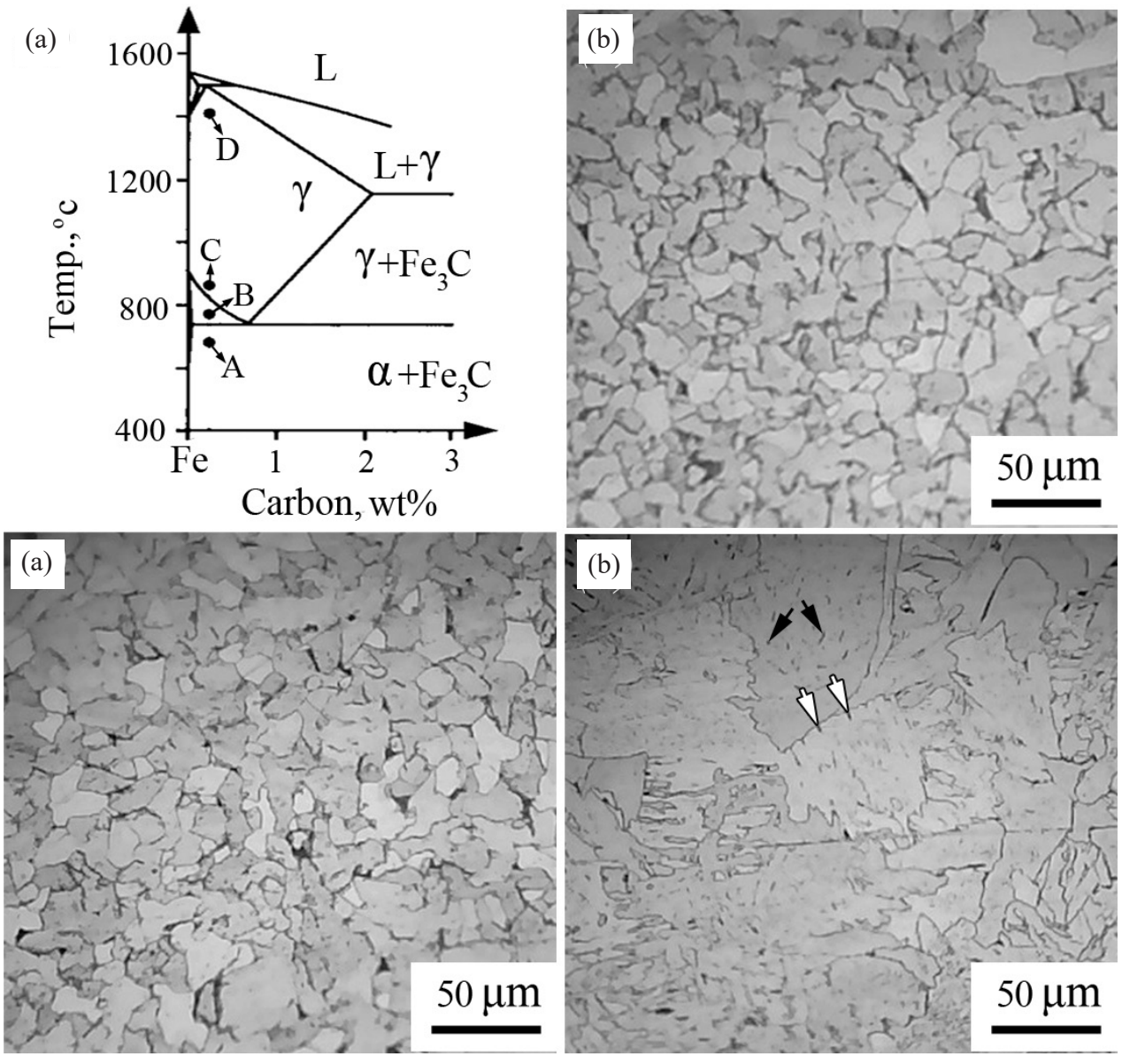

Fig. 2. (a) Fe–C phase diagram showing the peak temperature for different parts of HAZ, (b) the partially grain refining, (c) grain refining, and (d) grain growth zone.

Fig. 3 shows the microstructure of stainless steel BM and the interface of HAZ with weld metal of the specimen welded with 100 A. The BM (Fig. 3 (a)) consists of equiaxed austenite grains with an average grain diameter of 35 ± 2 µm. The microstructure of HAZ does not show a significant grain growth. The HAZ is not very wide due to the low heat conduction coefficient and also the high heat capacity of AISI 316L. The size of the HAZ grains does not increase rapidly with approaching to the welding zone, because the delta ferrite formation in the austenite grain boundaries at high temperatures limits the austenite grain growth [15]. The average diameter of grains in this area is 37 ± 2 µm, which does not have a significant difference compared to the BM. In this area, there is a slight possibility of formation of Cr carbides which are precipitated at the grain boundaries and reduces the corrosion resistance by reducing the Cr content in the adjacent area [5]. The other joints welded with different curents have a similar microstructure.

In the fusion zone (Fig. 3(b)), the delta ferrite can be seen between the austenite dendrites and cells adjacent to the HAZ. Due to the fact that the BM and the electrode have the same chemical composition and crystalline structure, the epitaxial growth occurs in the weld-HAZ inteface [13].

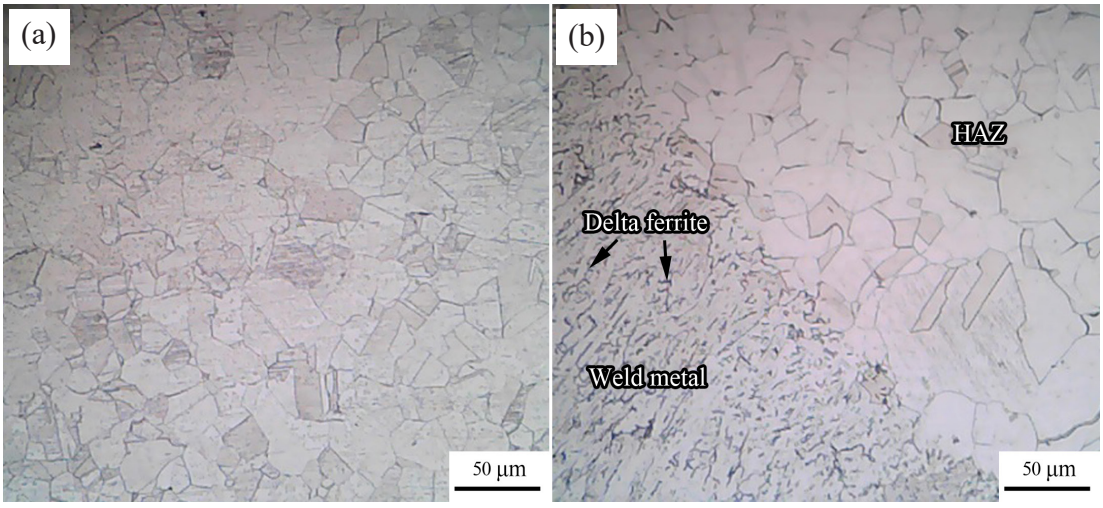

Fig. 3. The microstructure of (a) AISI 316 BM and (b) interface of HAZ of AISI 316 steel and the weld metal.

Fig. 4 shows EDS line scan from the transition zone between the stainless steel and the weld metal. By going from the St-37 to the AISI 316, there is an increase of Cr and Ni content. As it can be seen, these elements diffuse along the joint and produce a metallurgical joint. The width of this area is less than about 20 µm.

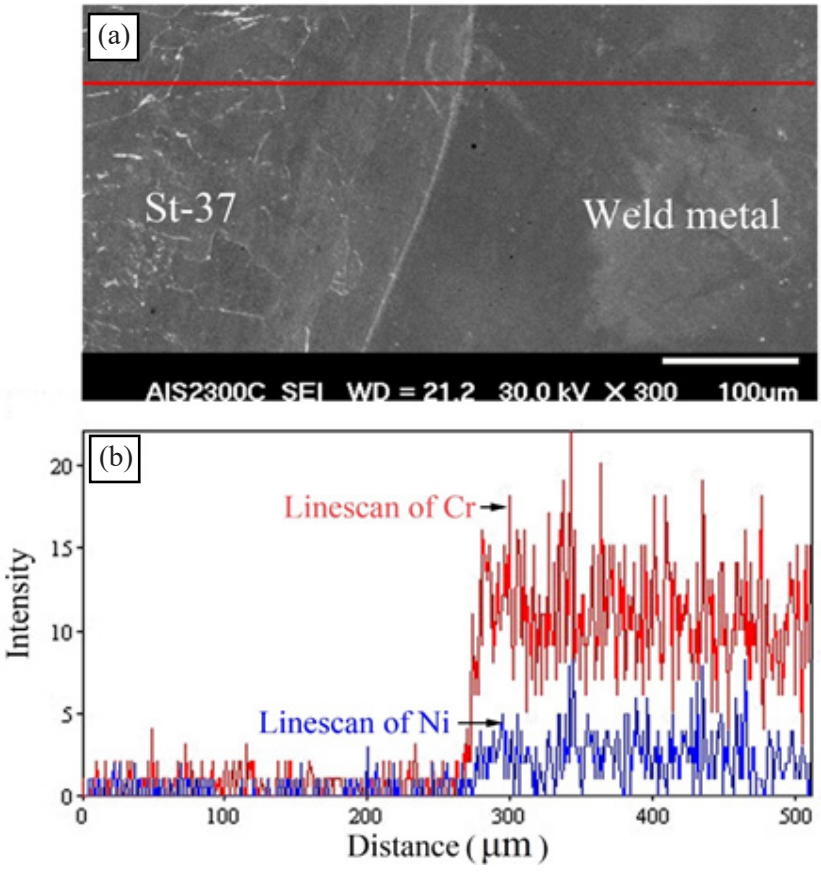

Fig. 4. (a) SEM micrograph of interface of St-37 and weld metal, (b) and (c) EDS linescan results of Cr and Ni across red line in part (a).

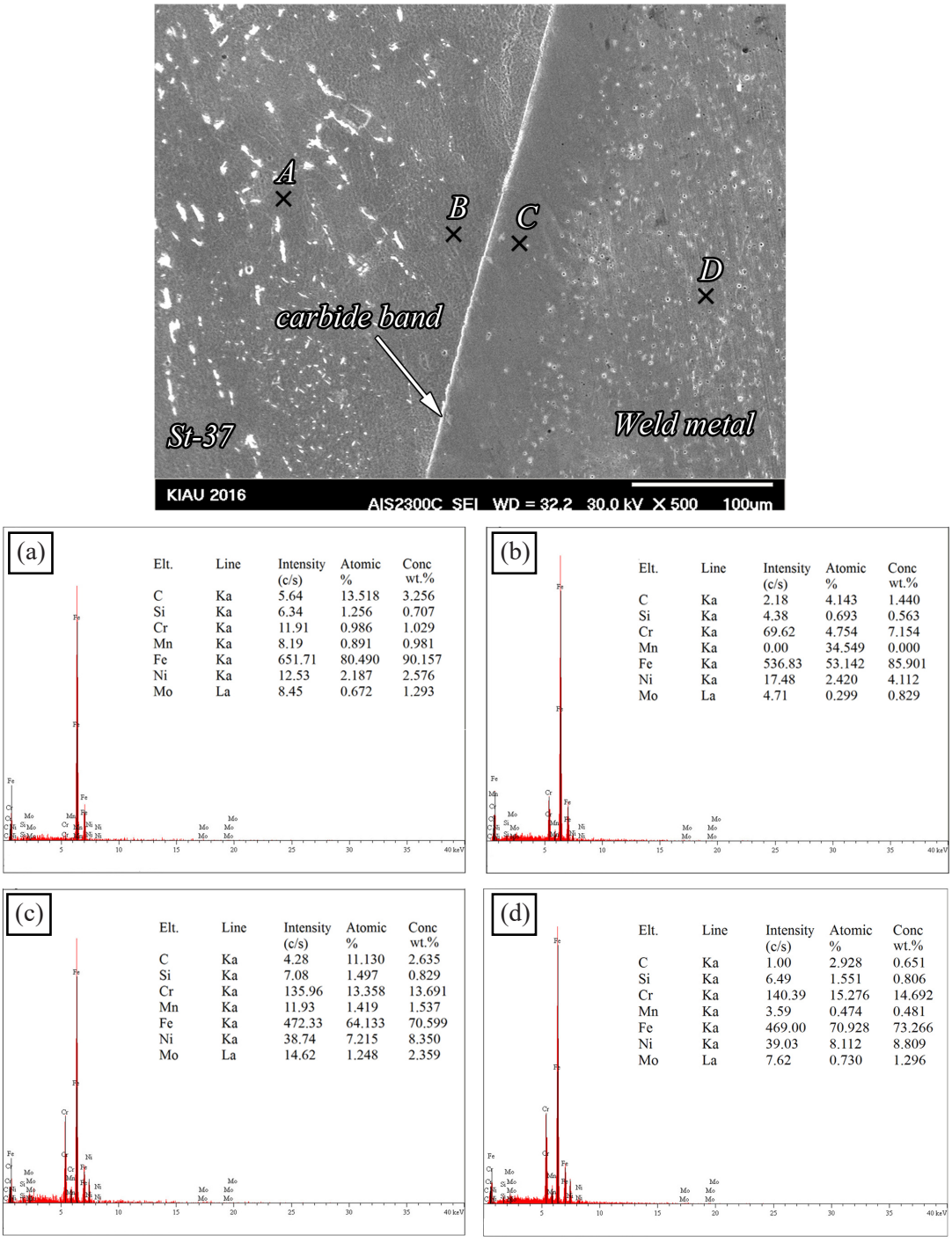

Fig. 5.Top part: SEM micrograph from the interface of St-37 steel and weld metal. EDS results from (a) St-37 HAZ (point A), (b) carbon-depleted zone (point B), (c) transition region (point C) and (d) weld metal (point D).

The upper part of Fig. 5 shows the SEM micrograph from the interface of St-37 and weld metal produced with 100 A current. One of the phenomena that occurs during welding, heat treatment, and under working conditions for this type of bonding, is the carbon migration from low-carbon steel to the welding zone. This creates a carbon-poor region (Carbon Depleted Zone, CDZ) in the HAZ of low carbon steel and in the vicinity of the fusion boundary. This carbon-poor region is prone to cracking [16]. The process of carbon migration involves the dissolution of carbides in the ferritic steel and the penetration of carbon into the welding pool [17]. The interface and grain boundary carbides has also been observed in diffusion bonding of AISI 304 to AISI 4140 steel [18].

In the welded joints between the dissimilar austenitic and ferritic steels, there is a transition region inside the welding pool and adjacent to the ferritic steel. Transition area in optical metallographic images is seen as an un-etched region due to the different chemical composition of this region from the weld metal [19]. Some researchers have reported the presence of martensite [20], and some others have declared the presence of carbide in this region [17]. That is the reason why this region is undesirable. There are some evidences about the damage initiation in this area [21,22].

The EDS results (Fig. 5(a) to (d)) show the amounts of Fe, Cr and Ni. By approaching from the St-37 BM to the weld metal, there is an increase of Cr and Ni elements and a decrease of Fe. The region A is according to the grain growth zone of St-37 steel and region B is the CDZ. As it can be seen, this region is free of cementite and has the lowest amount of carbon. The carbon of cementite dissolves and diffuses toward the weld metal. The Cr element also diffuses from the weld metal toward the St-37 steel. Therefore these elements produce Cr-rich carbide which can be seen as a white narrow band along the fusion line. The transition region (C) can be seen as an un-etched region. It has been reported that the unmixed region has a chemical composition similar to the BM [23], but this study shows the presence of about 8% Ni and 13% Cr in this region. It shows that the diffusion of Cr toward the St-37 steel has decreased the amount of this element and the Ni content is lower than the electrode. The authors suggests that this area has a chemical composition that the final microstructure is austenite - martensite, according to the Shaeffler shaeffler diagram. Region D shows that the weld metal has a lower Cr and Ni than the electrode, due to the dilution, but the microstructure of this area is austenite and delta ferrite, similar to the middle of the joints.

Fig. 6 shows the microstructure of the center of weld metal (100 A). The microstructure consists of delta ferrite dispersed in the austenitic background. The EDS result shows the chemical composition which is almost close to the E316L, but the Cr and Ni is decreased as a result of dilution. The microstructure contains austenite with some skeletal ferrite which shows that the weld metal has the solidification type FA, which the solidification begins with the formation of an initial ferrite, and a certain amount of austenite forms at the end of solidification. When the weld cooling rates are moderate or when the C_{req} / N_{ieq} ratio is low but still within the FA range, the skeletal ferrite morphology is formed. This is a consequence of the austenite front consuming the ferrite until the ferrite is sufficiently enriched in ferrite-stabilizing elements (Cr and Mo) and depleted from the austenite-stabilizing elements (Ni, C and N), therefore delta ferrite remains stable at lower temperatures where diffusion is limited [2].

Fig. 7 shows the microstructure of weld metals produced by different heat inputs. As it can be seen, the delta ferrite is decreased when the welding current or heat input increases. The amount of ferrite in the samples welded by heat inputs of 0.72, 0.84 and 1.0 kJ mm^{-1} equals to about 13, 9 and 5%, respectively. The reason is that when the heat input increases, the cooling rate decreases and as a result, the amount of austenite in the weld metal increases because there is more time for decomposition of delta ferrite to austenite.

In the welded joints between austenitic stainless steels and carbon steels, one of the most important factors that should be considered is the solidification cracking. The presence of delta ferrite in the weld metal is necessary to avoid cracking [24, 25]. It has been stated that the highest hot cracking resistance is achieved within the range of 5-20% ferrite [26]. The Schaeffler diagram can be used to predict the microstructure of the weld metal [2]. The Cr and Ni equivalent of BMs and electrode is calculated. Considering the 70% dilution for the BMs, the weld metal composition will be located between 5 and 10% iso-ferrite line. The resulting microstructure is two-phase

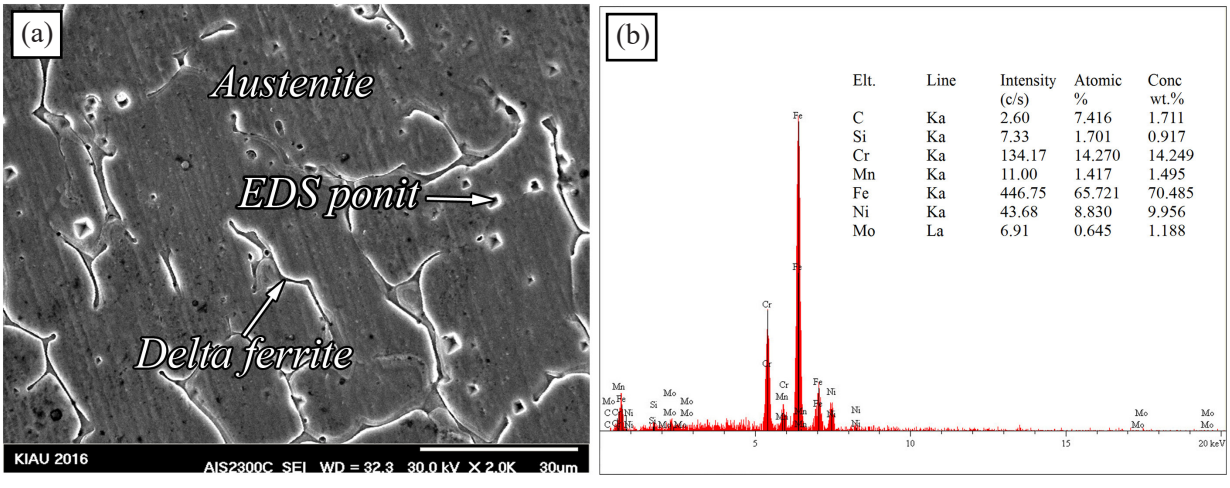

Fig. 6. (a) SEM micrograph of weld metal and (b) EDS results from the point in part (a).

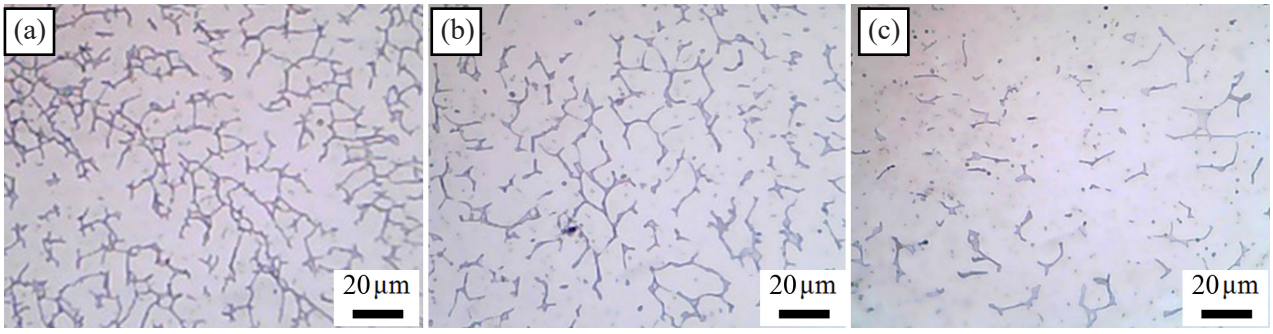

Fig. 7. Evolution of delta ferrite in the weld metals produced by different heat inputs: (a) 0.72, (b) 0.84, and (c) 1.0 kJ mm^{-1}.

(austenite-ferrite) alloy which is resistant to the solidification cracking. This is consistent with the results of image analysis.

In the welding of austenitic stainless steels, there is a possibility of σ phase formation at the ferrite-austenite boundaries due to the high Cr content at these regions [27,28]. No sing of σ phase was not found in the joints, because it needs a long time exposure at high temperatures.

3.2. Microhardness and Tensile results

The Vickers microhardness results is shown in Fig. 8 (a). The hardness of the St-37 and AISI 316L BM is about 100 and 170 HV. The partially grain refining and grain refining zones of St-37 steel has small grain of ferrite and P colonies which increases the hardness. In the grain coarsening St-37 HAZ, despite the growth of the ferrite grains, the hardness is increased, which is suggested to be due to the formation of Widmanstatten ferrite and dispersed cementite among ferrite boundaries.

The hardest region of the joints is close to the St-37 steel side, which is according to the region containing carbide and martensite. The existence of small martensitic zone with a high hardness is also has been reported in GTAW of austenitic stainless steel to low alloy steel [23].

The hardness of the weld metal is also close to the austenitic stainless steel. By increasing the welding current, the hardness of the samples decreases. This is due to an increase in the cooling time of the weld metal, which causes more austenite formation in the weld metal. The austenite is known as softer phase and it has been reported that the ferrite has higher hardness [29]. The hardness of the austenitic steel HAZ is similar to its BM, because the only change in this area is a slight grain growth and possibly the formation of small amounts of Cr carbide at the austenite grain boundaries.

The tensile properties of both BMs and the transversal tensile samples from each weld are listed in table 3. It should be noted that the failure in all transversal tensile samples occurred from the St-37 steel BM (weakest point of the welds), which is shown in Fig. 8b. The

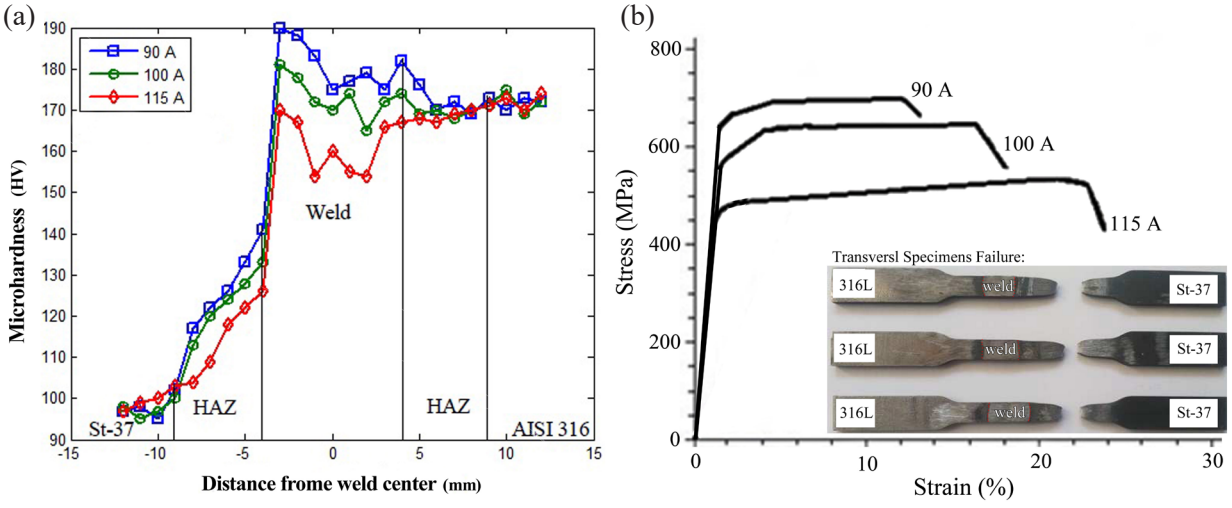

Fig. 8 (a) Microhardness profile along the cross-section of welds; (b) stress-strain curves of longitudinal tensile samples and the images of fractured transversal tensile samples.

Table 3. Tensile properties of BMs and transversal tensile samples.

Sample	UTS (MPa) *	Elongation (%)
St-37 BM	380±5	26±0.7
AISI 316L BM	570±7	42±2
Weld-90A	381±4	26±1
Weld-100A	377±6	28±1
Weld-115A	371±3	30±1

* Standard deviation for two samples

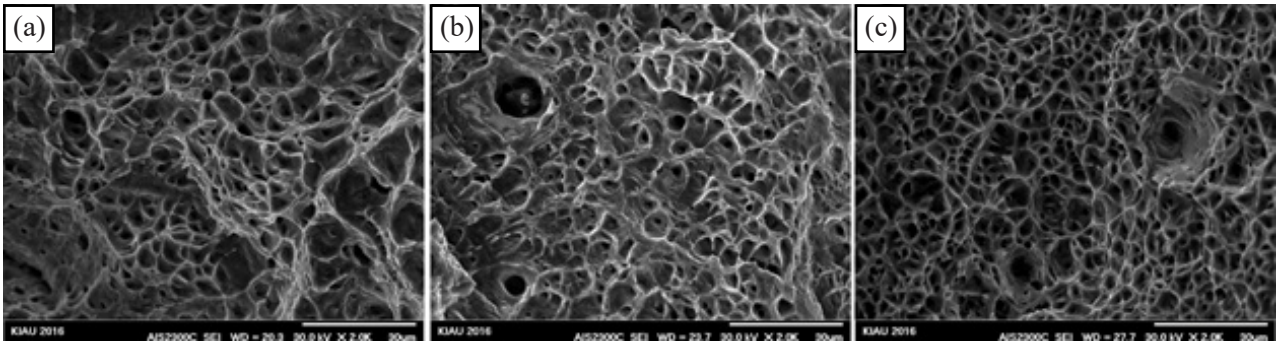

Fig. 9. SEM micrographs from fracture surfaces of different welds: (a) 90A, (b) 100A, and (c) 115A.

tensile strengths of the transversal samples is related to the strengths of the fracture points. The specimens fracture occurred in the St-37 BM, therefore the strength of the transversal samples is almost the same as the St-37 BM. The reason that the failure dose not occur at the carbon depleted zone is that this zone is narrow and it is near the carbide and martensite band with higher strength which can compensate the strength of this area. It can also be deduced that the carbon content in the st37 steel is low (0.08%); therefore reducing the carbon content is not so much and have a little effect of the strength.

Fig. 8 (b) also shows the engineering stress-strain curves of the longitudinal samples taken from each weld metal. The Austenitic stainless steels usually have a large elongation in tensile test [30]. As the heat input increases, the tensile strength decreases and the elongation increases. The fracture surfaces of the welds are shown in Fig. 9. The presence of many dimples at the fracture surfaces shows the ductile fractures. It has been pointed out that increasing the amount of ferrite would increase the tensile strength and with decreasing the heat input, the ferrite content of the weld metal will increase. Since the austenite is a ductile phase with a high elongation, the higher austenite content in the weld metal increases the ductility of the weld [31, 32].

4. Conclusions

- The St-37 HAZ region is divided into three regions of partially grain-refining, grain-refining, and grain-coarsening regions (coarse ferrite with Widmanstatten ferrite). The HAZ of AISI 316L steel shows only a little microstructural change and has a little grain growth.
- The weld metal has a solidification microstructure type FA containing austenite and delta skeletal ferrite. The amount of delta ferrite decreases from 13 to 5% by increasing the heat input from 0.72 to 1.0 kJ mm-1. This is due to the more time for $\delta \rightarrow \gamma$ decomposition.
- At the interface of carbon steel with the weld metal, the narrow carbide band is observed due to the migration of carbon from the St-37 steel HAZ toward weld metal. There is an unmixed region which is suggested have austenite-martensite structure.
- The hardness of the joints increases with decreasing the heat input. The Cr carbide and martensitic bands near the carbon steel has the highest hardness.
- The welds has higher strength compared to the St-37 BM. With increasing the heat input, the strength

of the welds decreases but their elongation increases. This is due to the decreasing of delta ferrite in the weld metals.

References

[1] A. Celik, A. Alsaran: Mater Charact, 43(1999), 311.
[2] JC. Lippold, DJ. Kotecki: Welding metallurgy and weldability of stainless steels, John Wiley & Sons, New Jersey, (2005), 287-306.
[3] H.S. Kim, J. Shin, B.S. Kong, S. Hong, S. Oh, J.D. Hong, C. Jang, S. Lee: Int J Press Vessel Pip, 172(2019), 17.
[4] D.K. Singh, G. Sahoo, R. Basu, V. Sharma, M.A. Mohtadi-Bonab: J Manuf Process, 36(2018), 281.
[5] M.P. Reddy, A.A.S. Aldrin, M. Prashanth, S.N. Kumar, K. Ramkumar, N. Arivazhagan, S. Narayanan: Procedia Eng, 75(2014), 29.
[6] A.R. Khalifeh, A. Dehghan, E. Hajjari: Acta Metallurgica Sinica, 26(2013), 721.
[7] M.J. Torkamany, J. Sabbaghzadeh, M.J. Hamedi: Mater Des, 34(2012), 666.
[8] H. Isazadeh, J. Bunn, H. E. Coules, A. Achuthan, J. Goldak, D. K. Aidun: Weld J, April(2016), 111.
[9] N. Arivazhagan, S. Singh, S. Prakash, G.M. Reddy: Mater Des, 32(2011), 3036.
[10] P. Kumar, A.N. Sinha: Lasers in Manufacturing and Materials Processing, 5(2018), 317.
[11] A.H. Khosrovaninezhad, M. Shamanian, A. Rezaeian, M. Atapour: J Adv Mater, 34(2015), 89.
[12] S Murugan, Sanjai K Rai, P. V Kumar, T Jayakumar, Baldev Raj, M.S.CBose: 78(2001), 307.
[13] S. Kou: Welding Metallurgy, Johan Willy and Sons, New Jersey, USA, (2003), 37-64.
[14] ASME. Qualification standard for welding and brazing procedures, welders, brazers and welding and brazing operators. ASME Boilers and Pressure Vessel Code, Sec IX ASME; 2006.
[15] A. Shahhosseini, F. Kermanpur, M. Shamanian: Mater Charact, 62(2011), 25.
[16] C. Lundin: Weld J, 61(1982), 58.
[17] S. Wang, Q. Ma, Y. Li: Mater Des, 32(2011), 831.
[18] B. Kurt: J Mater Process Technol, 190(2007), 138.
[19] B.I. Mendoza, Z.C. Maldonado, H.A. Albiter, P.E. Robles: Scientific Research, 2(2010), 520.
[20] E. Barnhouse, J. Lippold: Weld J, 77(1998), 477.
[21] G. M. Fallatah, K. S. Anwar, K. Zafarullah, J. K. Boah: The 6th Saudi Engineering Conference, (2002), 297-312.
[22] C. Pan, Z. Zhang: Mater Charact, 36(1996), 5.
[23] I. Hajiannia, M. Shamanian, M. Kasiri: Mater Des, 50(2013), 566.
[24] R. Saluja, K. M. Moeed: Int J Sci Eng Res, 7(2016), 493.
[25] S. Hong, H. Kim, B. S. Kong, C. Jang, I. H. Shin, J.S. Yang, K.S. Lee: Int J Press Vessel Pip, 167(2018), 32.
[26] E. Folkhard, G. Rabensteiner, E. Perteneder, H. Schabereiter, J. Tosch: Welding Metallurgy of Stainless Steels, Springer-Verlag, Wien-New York, (1988), 161.
[27] C. C. Hsieh, X. Guo, C. M. Chang, W. Wu: Met Mater Int, 16(2010), 349.
[28] C. C. Hsieh, T. C. Chang, D. Y. Lin, M. C. Chen, W. Wu: Met Mater Int, 13(2007), 411.
[29] R. Ghasemi, B. Beidokhti, M. Fazel-Najafabadi: Archive of Metallurgy Materials, 63(2018), 437.
[30] N. Singh, T. Nanda, B. R. Kumar, S. K. Das, V. Singh: Arch Civ Mech Eng, 19(2019), 672.
[31] D. Hauser, J.A. Van: Weld J, 61(1982), 37.
[32] N. Taehoon, E. An, B. Kim, S. Shin, W.S. Ko, N. Park, N. Kang, J. Jeon: Metals, 8(2018), 26.